Corner spalling and tension stiffening in heat-damaged R/C members: a preliminary investigation

Francesco Lo Monte · Pietro G. Gambarova

Received: 6 February 2014 / Accepted: 26 September 2014
Published online: 05 October 2014

1 Introduction

Concrete, reinforcement and concrete-reinforcement bond are the three pillars of reinforced-concrete structures, with the concrete contributing to both the bearing capacity and the protection of the reinforcement, especially at high temperature and in fire conditions. While concrete and steel properties at high temperature are well known, and so bond properties concerning the anchoring ability (mostly involving equilibrium among steel, concrete and bond stresses), cover spalling (leading to the exposure of the reinforcement to the fire) and tension stiffening are still open to investigation. (Tension stiffening is the other face of bond involving the strain compatibility between concrete and steel).

F. Lo Monte · P. G. Gambarova (✉)
Department of Civil and Environmental Engineering (DICA), Politecnico di Milano, Milan, Italy
e-mail: pietro.gambarova@polimi.it

Fig. 1 Corner spalling in R/C members during a fire: **a** columns, and **b** beams

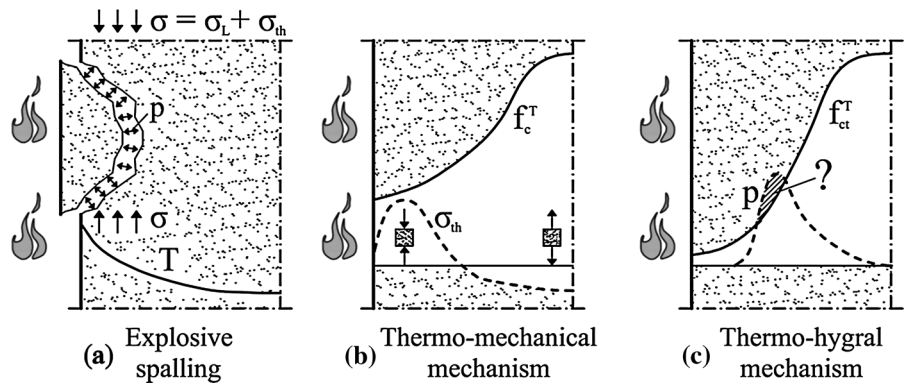

Fig. 2 Explosive spalling and typical temperature profile in a heat-exposed wall (**a**); plots of thermal stress σth and compressive strength f_c^T (**b**); and plots of pore pressure p and tensile strength f_{ct}^T (**c**); the question mark in **c** stands for the negative interaction between pore pressure and tensile strength

The heat-induced damage in the concrete [1] is mostly concentrated in the reinforcement cover, where the damage may exhibit different features, from hairlike cracking to discrete cracking, from scaling to more or less severe spalling, with aggregate splitting and/or enucleation [2]. In some cases spalling (that is the most severe form of damage [3–7]) is rather local and progressive as in the column shown in Fig. 1a; in other cases it is extended and explosive as in the beam shown in Fig. 1b. In unreinforced members, discrete cracks may form at right angles to the corners, mostly because of concrete desiccation. The different forms of damage, however, are rather elusive, since—depending on a number of parame-ters—one form or another may prevail in nominally-identical specimens, for no specific reasons. Hence, not only spalling as such has become a very hot topic, but standardized tests to assess the spalling sensitivity of the many cementitious composites available today are badly needed. The tests should be as simple, reproducible and general as possible, with the least possible number of parameters, beside those related to the thermal field and to concrete constitutive behavior (Fig. 2). The setting should be rather demanding (for instance, a corner exposed to the fire) and the fire scenario should be rather severe (for instance hydro-carbon fire), in order to activate pore pressure [1, 8, 9] (Fig. 2c) and aggregate splitting. At the same time, thermal self-stresses (Fig. 2b) and load-induced stresses (Fig. 2a) should be ruled out or kept to a minimum, since they depend on the structural context.

With reference to tension stiffening, it is worth recalling that the flexural cracks cause the unloading of the concrete at the cracked interface, and the

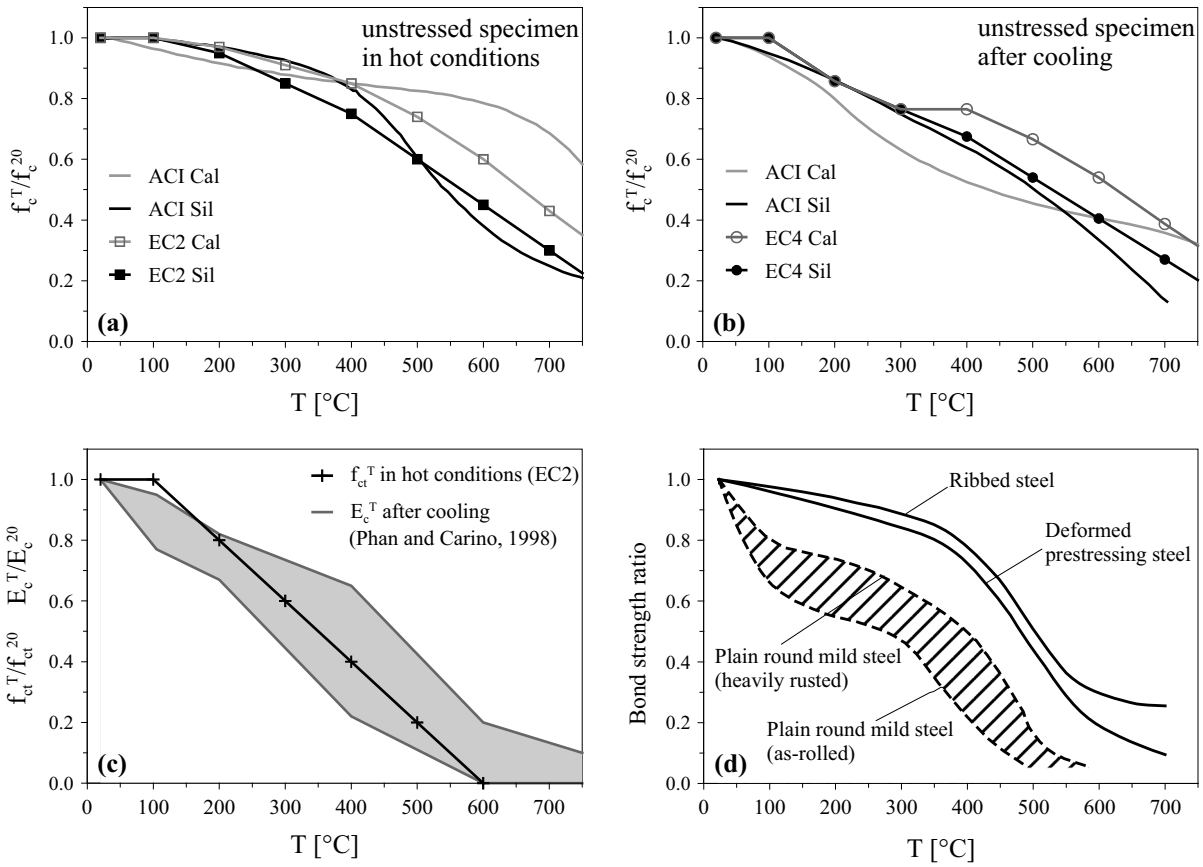

Fig. 3 Normalized plots as a function of the temperature: **a** hot compressive strength of unstressed specimens according to ACI [13] and EC2 [14]; **b** residual (after cooling) compressive strength of unstressed specimens according to ACI [13] and EC4 [16]; **c** hot tensile strength according to EC2 [14] and secant modulus [17]; and **d** bond strength in hot conditions ([12]; see also RILEM, 1985 [10])

increase of the tensile stresses in the reinforcement. Between two contiguous cracks, the bond stresses are responsible for the partial unloading of the bars and for the partial loading in tension of the surrounding concrete. Hence, any embedded bar—being *relieved* by the concrete—exhibits a *stiffer* behavior compared to a similar naked bar. This is tension stiffening, that plays a considerable role in crack control and markedly affects structural stiffness.

As a matter of fact, since most concrete structures survive even severe fires, their repair and rehabilitation should be devised to guarantee not only the bearing capacity, but also the control of the displacements, that depends on materials residual stiffness, residual steel–concrete bond and tension stiffening.

Since tension stiffening is related to bond, tension stiffening and fire should be examined within the context of bond and high temperature. Bond versus high temperature was extensively studied in the eighties of the past century [10], with reference to the effects of: mix design, aggregate type, curing conditions, shape/size/surface conditions of the reinforcement, shape of the specimens and test procedures. Beside the great difference between smooth and deformed bars, the roughness of the reinforcement, the aggregate type, the testing procedure (at high temperature/in residual conditions), the curing conditions and the shape of the specimen were recognized as being the major factors controlling bond at high temperature. Bar roughness, calcareous aggregates, air curing (of the concrete) and high temperature (compared to residual conditions) bring in a better bond behavior in the heat-exposed reinforcement. Other topics, like the effect of metallic and polymeric fibers, and the role of

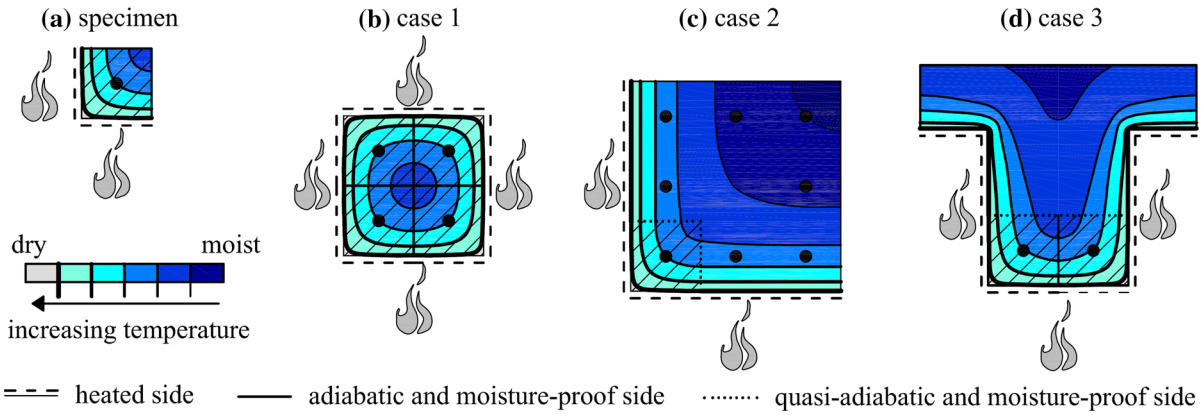

Fig. 4 Cross sections and hygro-thermal boundary conditions: prismatic specimen tested in this study (**a**); four-side heated column (**b**); two-side heated column (**c**); and typical beam (**d**). The colors refer to moisture content; the continuous curves are the isotherms

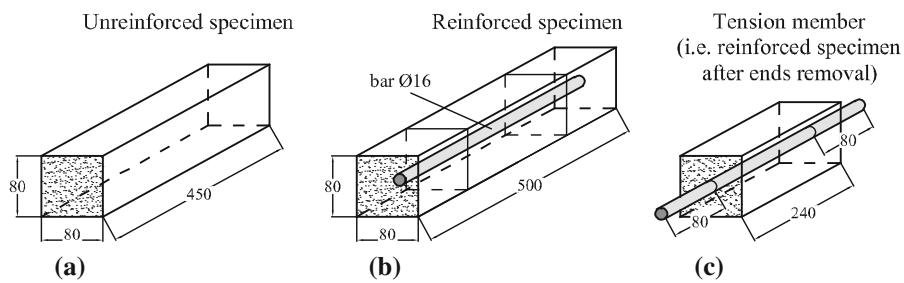

Fig. 5 Geometry of the unreinforced (**a**) and reinforced (**b**) specimens used to investigate spalling; and geometry of the reinforced tension members used to investigate tension stiffening after the removal of concrete cover at both ends (**c**)

Table 1 Mix design of the three self-compacting concretes

Concrete no. and type	NSC	HPC	HSC
Cement type	II/A-LL 42.5	I 52.5	I 52.5
Cement content (c) (kg/m^3)	350	480	520
Calcareous filler (kg/m^3)	130	100	100
Acrylic superplasticizer/ cement (%)	1.2	2.0	2.0
Water (kg/m^3) (w/c)	175 (0.50)	168 (0.35)	172 (0.33)
Aggr.: natural round river gravel d_a (mm)/mass (kg/m^3)	16/1,700	16/1,600	16/1,600
Mass per unit volume (kg/m^3)	2,359	2,358	2,402
Compressive strength: target/actual (MPa)	50/51	80/82	90/90

The denominations NSC (Normal-Strength Concrete), HPC (High-Performance Concrete) and HSC (High-Strength Concrete) are used only to facilitate the identification of the three materials in the text

expanded clay for large/medium aggregate, have been reconsidered lately [11].

To give an idea about bond decay at high temperature, the normalized bond strength is plotted in Fig. 3d [10, 12] as a function of the temperature, for smooth and ribbed bars, as well as for deformed prestressing reinforcement. It should be observed that bond decay in ribbed/deformed bars at high temperature ("hot" conditions) seems to be close to concrete decay in compression below 400 °C (Fig. 3a, [13, 14]) and to concrete decay in tension above 400 °C (Fig. 3c, [14]).(For recent data on concrete behavior at high temper-ature, see [15]; for the normalized compressive strength and the secant modulus after cooling, see Fig. 3b [16] and Fig. 3c [17], respectively).

Since the late eighties of the past century, limited attention has been given to bond and high temperature or fire, and only half a score of valuable papers can be found in major magazines [18–23]. Hence, new information is needed, on both the anchoring ability

at high temperature and tension stiffening, including the risk of cover spalling. Within this context, the rather unpretentious project presented in this paper aims to yield some preliminary results (a) on the definition of an experimental procedure to assess the spalling sensitivity of a given concrete, and (b) on the evolution of tension stiffening in R/C tension members exposed to roughly 650 °C.

The prismatic specimens were made of three different self-compacting concretes (target strength $f_c = 50$, 80 and 90 MPa), whose behavior at high temperature was investigated within a rather comprehensive research project in 2006–2010 [24], with reference to: stress–strain law in compression, fracture and thermal properties, in *hot* and *residual* conditions.

2 Objectives

The objective of the first phase of this project is to investigate corner spalling in self-compacting concrete and to work out a proposal for the design of an experimental set-up aimed to investigate concrete sensitivity to spalling in fire under realistic conditions regarding the thermal gradients, the pore pressure and the moisture transfer (thermal and load-induced stresses are not a primary concern) [25]. Investigating tension stiffening is the objective of the second phase [26]. (A synthesis of both papers can be found in [27]). The prismatic specimens—and the test set-up—were designed to represent the rather severe hygro-thermal situation of a corner subjected to the heat flux coming from two directions at right angles, as in R/C columns and beams (Fig. 4). From the point of view of the heat flux in actual columns and beams, the internal faces of each of the hatched prisms depicted in Figs. 4b,c,d are in either adiabatic conditions (all faces in Fig. 4b and vertical face in Fig. 4d, because of the symmetries), or close enough to adiabaticity (both faces in Fig. 4c and horizontal faces in Fig. 4d).

One should observe that the specimens depicted in Fig. 4a are not aimed to represent the kinematic restraint along the adiabatic or quasi-adiabatic surfaces of the sections shown in Fig. 4b–d, because the focus is on corner spalling and on a realistic reproduction of the hygro-thermal field, that plays a major role in concrete spalling. The necessity of examining concrete spalling from the point of view of the material has been stressed in a number of recent papers and by well-known scholars [28, 29].

After being exposed to a thermal shock to produce spalling (with the introduction of the reinforced/unreinforced specimens into a furnace pre-heated to 750 °C, Fig. 5a, b), the specimens were left at 750 °C for 2 h in order to cause a rather uniform damage in the concrete. Then, after cooling down to room temperature, the unspalled reinforced specimens were reworked at their extremities (Fig. 5c), to allow the reinforcing bar to be loaded in tension at both ends, in order to investigate tension stiffening in residual conditions.

3 Specimens, materials and fire curve

Twenty-one prismatic specimens ($a \times b \times L = 80 \times 80 \times 450$–$500$ mm, Fig. 5) made of three

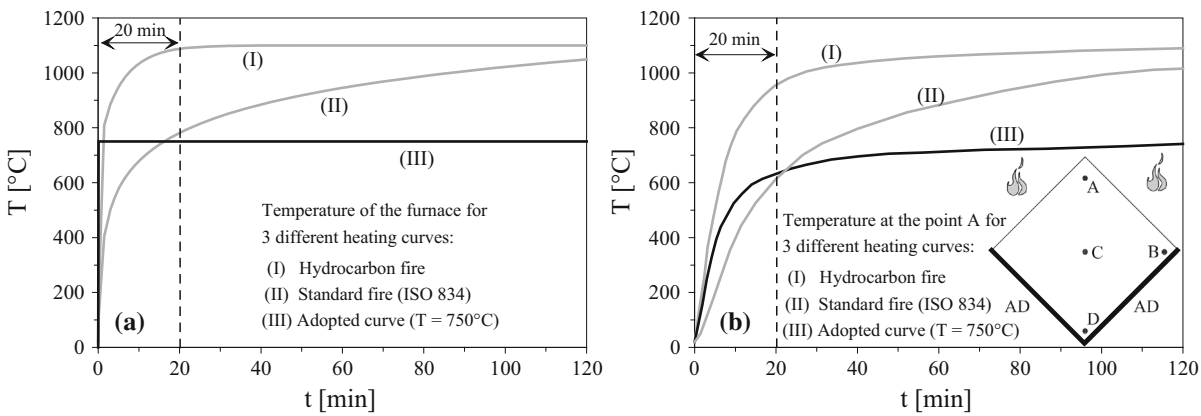

Fig. 6 **a** Plots of the hydrocarbon and standard fire curves (I, II) and of the curve adopted in this project (III); and **b** temperature evolution in point A (10 mm from each heated face) according to the three fire curves (I, II, III); *AD* = quasi-adiabatic surfaces

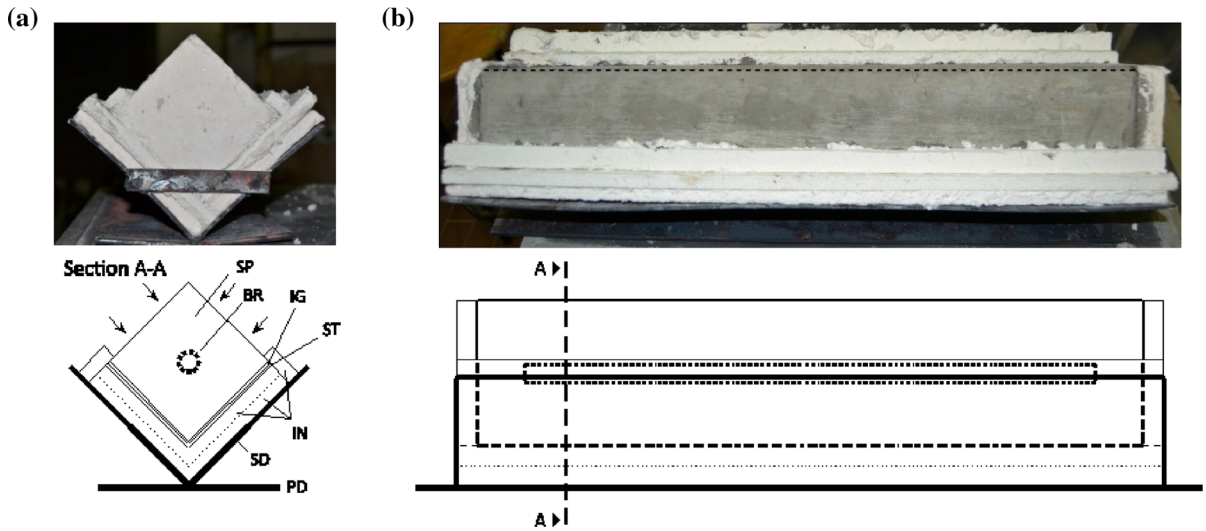

Fig. 7 Typical specimen placed on the saddle-like support and ready to be introduced inside the furnace: front (**a**) and lateral view (**b**); *SP* specimen, *BR* bar, *IN* insulating plate, *IG* impregnating coating + glue, *ST* steel barrier, *SD* V-shaped supporting saddle, and *PD* pedestal

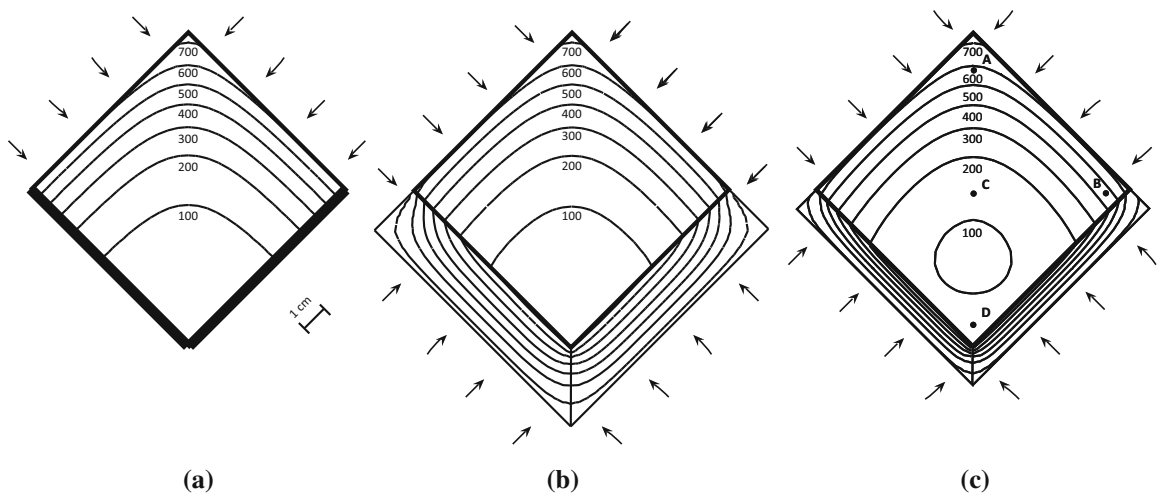

Fig. 8 Thermal analyses (performed by means of ABAQUS) 15 min past the introduction of the specimen inside the furnace at 750 °C: **a** adiabatic unexposed faces; **b** insulated unexposed faces, as in standard specimens; and **c** partially-insulated unexposed faces, as in Specimen HPC/P/D/2, which was instrumented with four thermocouples placed in A, B, C, D. The thermal properties of the concrete were those indicated in EC2 [14]

different self-compacting mixes (Table 1) were cast. Eleven specimens were reinforced with a single hot-rolled 16 mm-bar (close to #5, made of carbon steel with $f_y = 400$ MPa, $f_{yk} = 373$ MPa, Type FeB38 k according to the Italian Norms, $E_s = 205$ GPa).

Seventeen specimens were "standard" specimens, as will be explained later, while two unreinforced and two reinforced specimens were "preliminary" specimens, slightly different from the standard specimens in terms of insulation, instrumentation and/or heating procedure (for more details, see [25]). Since the focus was (a) on corner spalling because of pore pressure, and (b) on tension stiffening as such, the specimens were unstressed during the heating process (= no loads applied inside the electric furnace) and also the thermal self-stresses were reduced to a

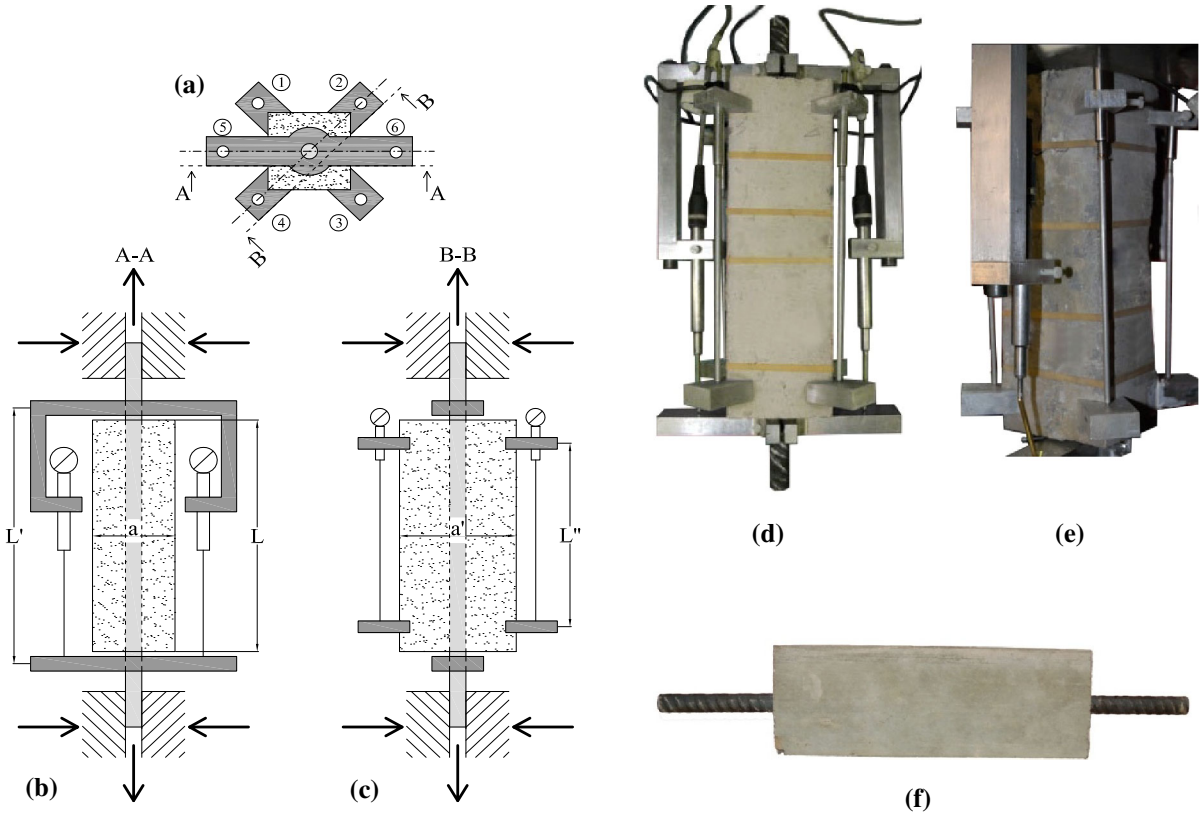

Fig. 9 Instrumented specimen ready for a tension-stiffening test: **a** cross section; **b**, **d** lateral view with the two LVDTs applied to the *bar*; **c**, **e** lateral view with two of the four LVDTs applied to the *corners*; and **f** typical specimen before testing; $L = 240$ mm; $L' = 270$ mm; $L'' = 180$ mm; $a = 80$ mm; $a' = 113$ mm

minimum, thanks to the rather small size and boundary conditions of the specimens.

Cylinders, cubes and prisms were cast in 2007 and appropriately cured for 28 days; then, in 2007–2009 the various specimens were tested in compression and indirect tension (by bending and splitting), generally in both hot and residual conditions, to work out the stress–strain laws in compression, and to evaluate the compressive and tensile strengths, as well as the fracture energy [15]. The conclusion of the previous study on SCCs' mechanical properties at high temperature was that there are no systematic and sizable differences with respect to ordinary concrete. Twenty-one prisms, and several cubes and cylinders were put aside and kept in ordinary environmental conditions ($T = 15$–25 °C; R.H. = 50–70 %), for further investigations on spalling and tension stiffening (2011 and 2012).

At the beginning of this project, the moisture content was close to 1.0 % in NSC specimens, and close to 2.5–3 % in both HPC and HSC specimens. Later, some specimens were put in a 50 cm-deep water tank for 1 week and a few for 2 weeks. The final moisture content was 4 % in NSC, 4.5 % in HPC and 3.3 % in HSC. (There was hardly any difference between the moisture content after 1 week and after 2 weeks in water). All wet specimens were left in air for 24 h, before being insulated, fastened to a steel saddle and introduced into the furnace, as indicated in the next chapter. The initial moisture content was evaluated by drying several small plates ($80 \times 80 \times 20$ mm, NSC, HPC and HSC) for 24–48 h at 105 °C.

The added moisture content was evaluated by weighing the prismatic specimens before and after being placed in the water tank. Each specimen (and its

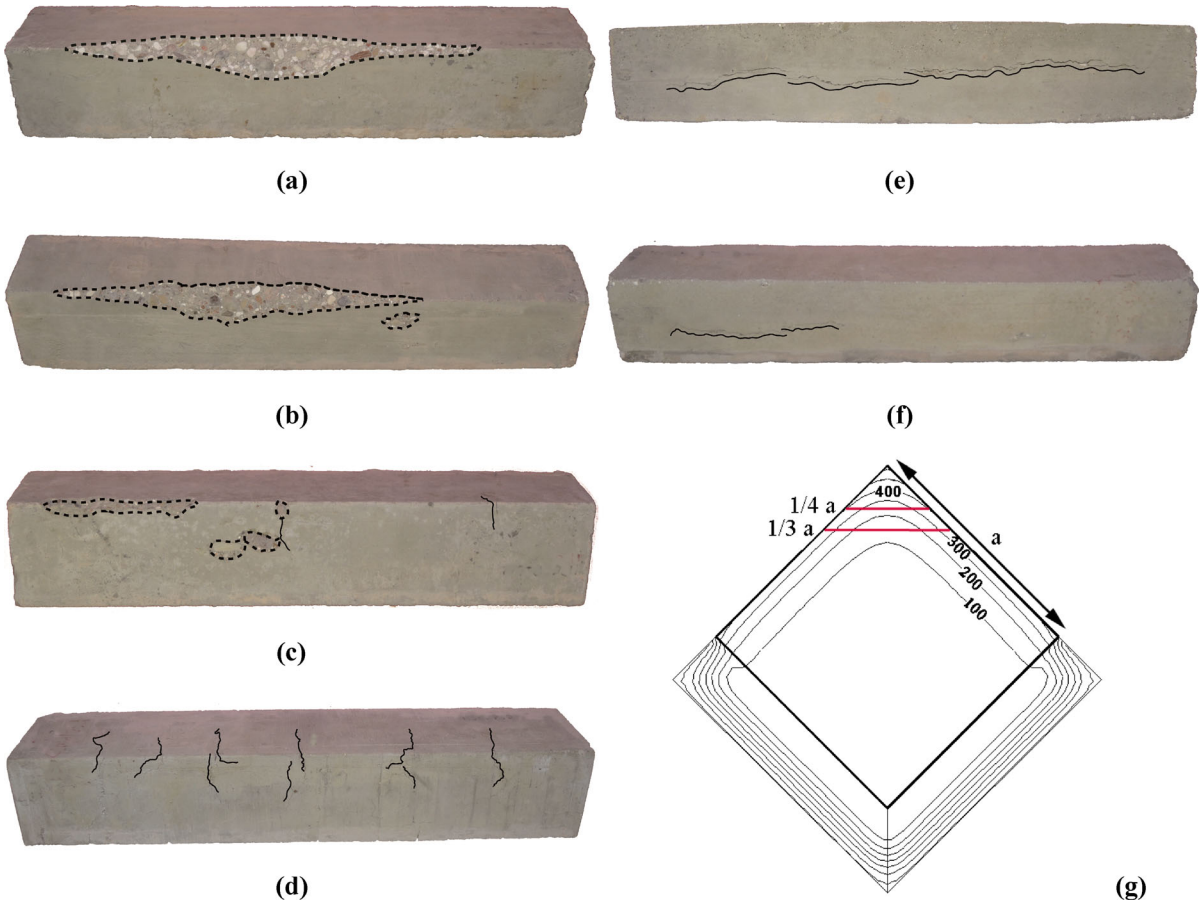

Fig. 10 Typical damage in unreinforced (**a**, **c**, **d**) and reinforced specimens (**b**, **e**, **f**) from the highest to the lowest damage level: **a** medium spalling in Specimen NSC/P/W/1; **b** medium spalling in Specimen HPC/R/W/1; **c** light spalling with some indentation and scaling in Specimen HPC/P/W/2; **d** light corner cracking in Specimen HSC/P/D/1; **e** fully-developed longitudinal cracking in Specimen NSC/R/D/1; **f** partially-developed longitudinal cracking in Specimen NSC/R/W/1; and **g** thermal field at the onset of spalling and typical spalling depth

saddle-like support, as explained later) was introduced inside an electric furnace kept at the nominal temperature of 750 °C (min. 740 °C, max. 780 °C), in order to let the surface temperature increase (in the first 20 min) in a way intermediate between those ensuing from the hydrocarbon fire curve and from the standard fire curve, respectively (Fig. 6). It was a sort of thermal shock intended to create the most favourable conditions for spalling. After the first 20 min and in the next 100 min, the thermal field progressively became homogeneous, with the final mean temperature being close to 640 °C. The specimens were identified by means of an alpha-numeric code consisting of three letters (NSC, HPC, HSC) for the mix; one letter (P, R) for plain/reinforced concrete; one letter (D, W) for dry/moist concrete (1–2.5 % or 3.5–4.5 % by moisture mass); and one number ($\leq$4) identifying each nominally-equal specimen. Hence, for example, HPC/P/D/2 means 2nd dry unreinforced specimen made of high-performance concrete.

4 Test set-up and thermal field

4.1 Spalling

Each prism was exposed to high temperature (Fig. 6b) on the two faces defining a corner, while the other two faces and the end sections were kept in roughly adiabatic conditions (by means of proper insulation,

Figs. 7, 8). In this way, the thermal field of the prism coincides with that of a quarter of a square column (side 160 mm), while the kinematic field is in principle different, because the planarity of the adiabatic faces is not guaranteed (something that is guaranteed by symmetry in a column exposed on four faces). To avoid any moisture transfer across the adiabatic surfaces, their permeability was greatly reduced by impregnating the unexposed surfaces with a temperature-resistant silicate-based coating (thick-ness = 1 mm). After gluing thin metallic sheets (*barriers*) to the impregnated surfaces (thick-ness = 1 mm), each specimen was placed on a metallic V-shaped saddle, by interposing one or two insulating plates containing ceramic fibers (thickness of each plate 10 mm); similar but smaller plates were used to insulate the end sections (Fig. 7).

Later, the system saddle + insulated specimen was introduced into the furnace. The total weight of the system was close to 16 daN. (After opening the door of the furnace, the operator could easily and safely introduce the saddle and the specimen, and push it with a special rod in the proper position, inside a sort of steel cage fixed to the floor of the furnace, to prevent the electric coils from being damaged by the flying debris resulting from concrete spalling).

As previously mentioned, the specimen was left inside the furnace for 2 h at 750 °C; then the electric power was switched off and the furnace started cooling naturally, until the extraction of the specimen (300 °C). Then the furnace was brought back to 750 °C to allow the introduction of another specimen. In this way, the thermal ups and downs of the furnace were minimized. After the extraction from the furnace, the specimens were wrapped in an insulating blanket, until they cooled down to ambient temperature. The effectiveness of the insulating system (between the specimen and the saddle) was checked by inserting four thermocouples in Specimen HPC/P/D/2, which had only one 10 mm-thick insulating plate (Fig. 8c, points A, B, C and D). The experimental values of the temperature were in satisfactory agreement with the predictions of thermal analyses. (For instance, 15 min past the introduction of the specimen into the furnace, the actual temperatures in A and D were 540 °C and 140 °C, respectively, i.e. 9 % lower and 13 % higher than those predicted numerically). In all other specimens (*standard specimens*) two insulating plates were used (Fig. 8b) and the isothermal lines turned out to be very close to those evaluated by assuming perfect adiabatic faces against the saddle (Fig. 8a).

Last but not least, it is worth noting that the heat-exposed faces of each prism were (a) the bottom face and (b) one of the vertical faces during concrete casting, the two of them being against the formwork. (In this way, the two impregnated faces included the top face during concrete casting, where the effect of segregation brings in more porosity and finer aggregates).

4.2 Tension stiffening

As will be explained later, the majority of the eleven reinforced specimens exhibited some scaling and indentation during the thermal shock, and only a few underwent medium spalling. One specimen, however, was so badly damaged after the thermal cycle (Specimen NSC/R/D/1, severe longitudinal cracking on one face, see Fig. 10e), that could be used only to check the loading set-up and the instruments to be used in the tension-stiffening tests. Among the other ten specimens, three were made of NSC, four of HPC and three of HSC. After clearing the extremities of the specimens (Fig. 5c), each concrete prism was 240 mm long and the bar protruded by 80 mm at each extremity. Such a free length was sufficient to clamp the bar between the top and bottom hydraulic jaws of the electro-mechanical press Schenk (capacity 1,000 kN). All tests were displacement-controlled. Note that the length of each concrete prism ($L = 240$ mm $= 15\varnothing$) is comprised between the values of crack spacing $S_{cr,max}$ in R/C beams (BM) and tension members (TM), see EC2—Part 1–1 (2004) [30]:

$$\begin{aligned} S_{cr,max} &= k_3 c + k_1 k_2 k_4 (\varnothing/\rho_{p,eff}) \\ &= 195 \text{ mm(BM)} - 282 \text{ mm(TM)}, \end{aligned} \quad (1)$$

where $k_1 = 0.8$ (ribbed bars); $k_2 = 0.5$ or 1.0 in pure bending or tension); $k_3 = 3.4$; $k_4 = 0.425$; $c =$ net cover = 32 mm; $\varnothing = 16$ mm; $\rho_{p,eff} = 3.1$ %. (Note that $L = 15\varnothing$ may seem too small to investigate tension stiffening, but this is not the case, as the very good bond properties of both SCC and deformed reinforcement in ordinary environmental conditions guarantee a sizable tension-stiffening effect even on rather short embedments).

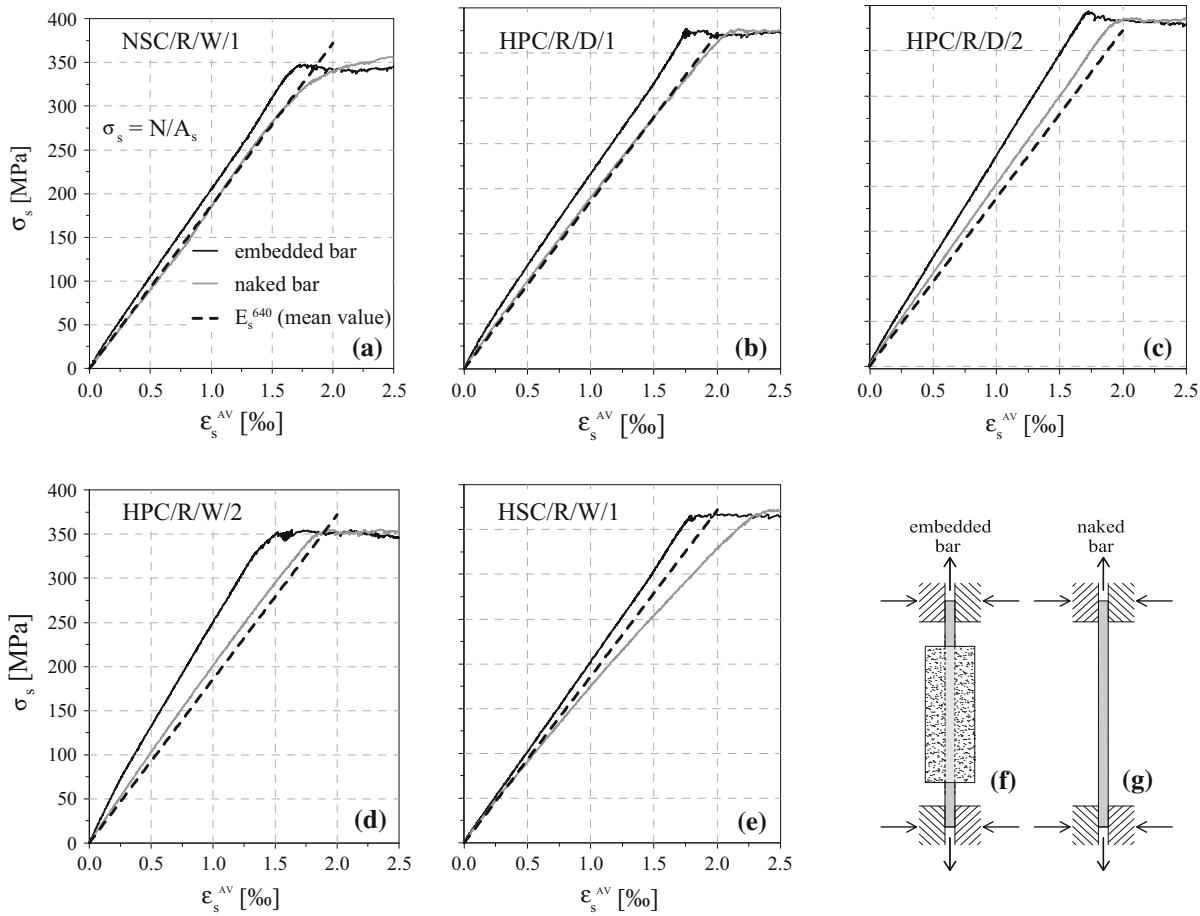

Fig. 11 Stress–strain curves of the five specimens exhibiting a sizable tension stiffening (**a**–**e**); and tests on embedded (**f**) and naked (**g**) *bars*. (ε_s^{AV} is the mean strain measured by LVDTs 5 and 6, Fig. 9a,b)

Four LVDTs were placed along the corners (Fig. 9), with base length $L'' = 180$ mm, to measure the mean elongation of the concrete, cracking included (if any). Two aluminum cross bars were fixed to the reinforcing bar close to the extremities of the concrete prism, in order to allow the placement of two LVDTs (base length $L' = 270$ mm) to measure the mean elongation of the bar. Later, after removing the concrete, each *naked* bar was tested in tension, to have the stress–strain curve in residual conditions (past heating to 640 °C), and to evaluate the strength at yielding and the elastic modulus. Unfortunately, no *reference* specimens were available to carry out the tests in virgin conditions (no heating).

Among the ten tests, that were successfully carried out, only five exhibited some tension stiffening, probably because the heat-induced damage at 640 °C was so severe that in some cases there was hardly any bond left.

5 Results

5.1 Spalling

A close examination of the twenty-one reinforced/unreinforced dry/moist specimens allows to subdivide the damage after the thermal cycle in five broad categories, as shown in Fig. 10: no visible damage (15 % of the specimens); partial/extended longitudinal cracking (20–25 %); corner cracking (25 %); light scaling and/or indentation of the corners (25–30 %); and medium spalling (10 %).

In detail:

- *Unreinforced dry specimens* (moisture content from 1 % in NSC to 2.5–3 % in HPC/HSC): very light scaling in NSC; some corner cracks in HPC and HSC, from hairlike to large (at least 0.5 mm wide); probably the higher moisture content—and the following desiccation—was responsible for the corner cracks in both HPC and HSC specimens.
- *Reinforced dry specimens* (same moisture content as in the previous case): single continuous longitudinal crack on one face of the exposed corner in NSC, with some scaling and indentation along the corner; practically no visible damage along the corner and on both faces in HPC and HSC specimens.
- *Unreinforced moist specimens* (moisture content from 3.3 % in HSC to 4 % and 4.5 % in NSC and HPC, respectively): medium spalling with aggregate splitting and enucleation in NSC; light spalling, scaling, indentation and corner cracking in both HPC and HSC; on the whole, the heat-induced damage was rather light.
- *Reinforced moist specimens* (same moisture content as in the previous case): in general, light discontinuous longitudinal cracking on one or both faces; in one case (HPC) medium spalling with aggregate splitting and enucleation.

In the two worst cases (Fig. 10a, b), spalling occurred roughly 3 min from the introduction of the specimen into the oven. The thermal field after 3 min is shown in Fig. 10g, where the temperature of the fracture surface is comprised between 150 and 250 °C. (It is worth noting that pore-pressure peaks generally occur in this range [31]).

In specimens NSC/P/W/1 (Fig. 10a) and HPC/R/W/1 (Fig. 10b) the spalled volume (over the spalled region) was close to 2.5 and 3.5 %, respectively, with the extension along each side of the corner comprised between 20 and 30 mm (from 1/4 to 1/3 of specimen side; extension of spalling close to 70 and 60 % of specimen length).

Even if the data base is very limited, what appears is that exposing either unreinforced or reinforced *dry corners* to a severe fire tends to produce corner cracking in unreinforced HPC/HSC specimens and longitudinal cracking in reinforced NSC specimens, while the unreinforced NSC specimens and reinforced HPC/HSC specimens tested in this project were hardly damaged.

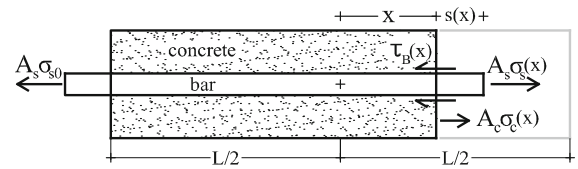

Fig. 12 Symbols and conventions adopted in the uni-dimensional slip-dependent model

In *moist corners*, spalling is an actual or impending occurrence, accompanied by some indentation and corner cracking, in both unreinforced (NSC) and reinforced (HPC) specimens; as in reinforced dry specimens, longitudinal cracking occurs in wet specimens as well, but in a rather limited form.

Last but not least, the very limited number of spalled specimens was unexpected. Some very recent test results, however, confirm that cover spalling—and particularly corner spalling—is not as likely to occur as one may expect, even in regions subjected mostly to tension [32]. (Only one of the nine continuous beams tested in [32] exhibited a limited and localized corner spalling under the standard ISO 834 fire; the moisture content—prior to heating—was comprised between 1.8 and 3.5 %, with a maximum close to 3.8 % in the spalled beam).

5.2 Tension stiffening

5.2.1 Experimental results

Five of the ten tests, that were successfully carried out on reinforced prisms, exhibited some tension stiffening, probably because the heat-induced damage at 640 °C was so severe that in 50 % of the cases there was hardly any bond left. After each test, the concrete was removed and the bar was tested in tension to work out its stress–strain law including the heat-induced damage at 640 °C. Then, comparisons were made between *embedded bars* (with tension stiffening) and *naked bars* (no tension stiffening). In Fig. 11a–e the stress–strain curves of the five specimens are reported (black curves), together with the curves representing the behavior of each naked bar (grey curves) and the dashed lines, whose slope is the mean value of the elastic modulus of the naked bars ($E_s^{640} = 186$ GPa). Note that σ_s is the nominal stress in the bar, N/A_s, and ε_s^{AV} is the mean strain measured by LVDTs 5 and 6 (Fig. 9a, b). With reference to Specimens

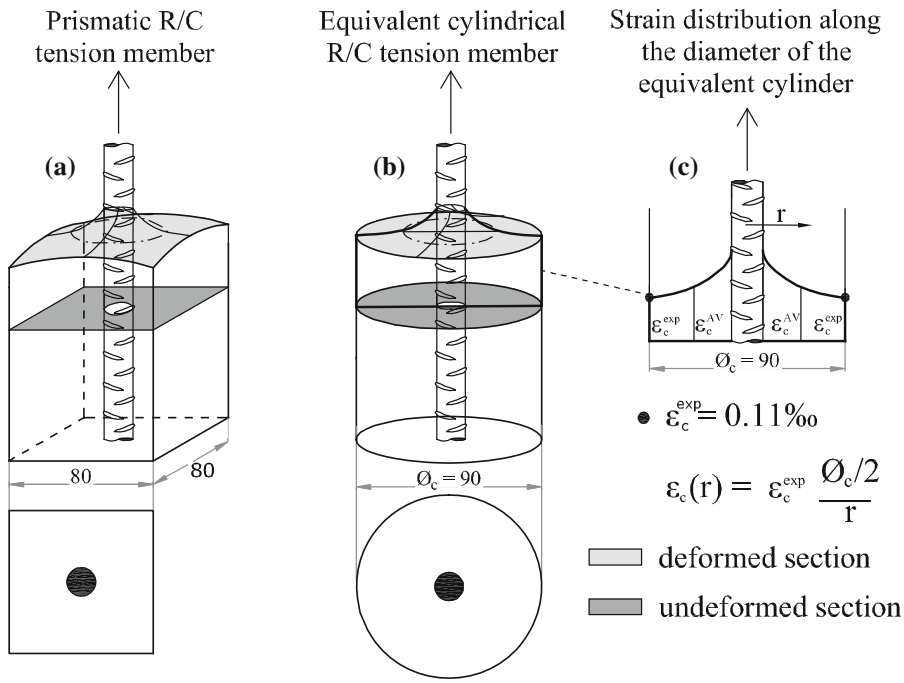

Fig. 13 Specimen HPC/R/D/1: deformed and undeformed cross-sections of the prismatic and of the equivalent cylindrical specimens (**a**, **b**); and mean profile of the normal longitudinal strain assumed in the analysis, for $N/N_{max} = 95$ % (**c**)

NSC/R/W/1, HPC/R/D/1 (*reference specimen* in the following), HPC/R/W/2 and HSC/R/W/1, at 95 % of the maximum load ($N_{max} = 70$–75 kN, depending on the actual strength at yielding of the bars) the mean share of the load borne by the concrete is comprised between 10 and 17 % (23 % in Specimen HSC/R/W/1, where the rather low residual elastic modulus of the naked bar casts some doubts on the behavior of this specimen, Fig. 11e).

The elastic modulus of the heat-damaged steel was roughly 10 % lower than that of the undamaged steel ($E_s^{640} = 186$ GPa—mean value measured on 11 bars, compared to $E_s^{20} = 205$ GPa).

As for the elastic modulus of the three concretes after a thermal cycle at 640 °C, six $80 \times 80 \times 160$ mm prisms were tested in compression (two per each concrete mix), and the modulus E_c^{640} turned out to be close to 6.0 GPa (*stabilized modulus* comprised between 5.5 and 6.6 GPa, according to the Italian Standard UNI 6556-1978 [33]). Hence, in residual conditions the ratio of the elastic moduli E_s^{640}/E_c^{640} was roughly 30. Note that the six concrete prisms were cut out from as many unreinforced specimens ($80 \times 80 \times 450$ mm) belonging to the series of 10 unreinforced specimens investigated to get information on spalling in the first phase of this project.

5.2.2 *Uni-dimensional slip-dependent model*

In order to justify the rather limited *residual* tension stiffening found in the tests, the well-known uni-dimensional axisymmetric model based on bar slip is used in the following.

The main assumptions are:

- both the bar and the concrete are subjected to a uniaxial state of stress: $\sigma_s(x)$ and $\sigma_c(x)$;
- both materials behave linearly and elastically (E_s and E_c);
- all relevant quantities depend only on the longitudinal coordinate x (in the tension-stiffening problem, there is a symmetry with respect to the transverse mean plane and the origin of x is on this plane; L is the total length of the concrete + bar system);

- the bond stress–slip law is assumed to be linear $\tau_B(x) = k\ s(x)$, where k is the *bond stiffness* (or *bond shear modulus*).

The equation of bond and the boundary conditions are:

$$\frac{d^2 s(x)}{dx^2} - k\frac{\pi \varnothing}{E_s A_s}(1+n\rho)\cdot s(x) = 0 \quad \text{with } s(0) = 0 \text{ and } \sigma_s(L/2) = \sigma_{s0}, \tag{2}$$

where, s = bar-concrete slip; $\rho = A_s/A_c = 3.1$ %; $\varnothing$ = bar diameter = 16 mm; k = bond stiffness; $n = E_s/E_c$; and σ_{s0} = applied stress; see Fig. 12 for the symbols and the conventions.

The solution in terms of bar slip s and stresses τ_B, σ_s, σ_c is:

$$s(x) = \frac{\sigma_{s0}}{\lambda E_s}\frac{\mathrm{Sinh}(\lambda x)}{\mathrm{Cosh}(\lambda L/2)} \tag{3}$$

$$\tau_b(x) = k\frac{\sigma_{s0}}{\lambda E_s}\frac{\mathrm{Sinh}(\lambda x)}{\mathrm{Cosh}(\lambda L/2)} \tag{4}$$

$$\sigma_s(x) = \frac{\sigma_{s0}}{(1+n\rho)}\left[n\rho + \frac{\mathrm{Cosh}(\lambda x)}{\mathrm{Cosh}(\lambda L/2)}\right] \tag{5}$$

$$\sigma_c(x) = \frac{\rho\sigma_{s0}}{(1+n\rho)}\left[1 - \frac{\mathrm{Cosh}(\lambda x)}{\mathrm{Cosh}(\lambda L/2)}\right], \tag{6}$$

where $\lambda = \sqrt{k\frac{\pi\varnothing}{E_s A_s}(1+n\rho)}$ and the parameters E_s, E_c, n and k are a function of the maximum temperature reached during the thermal cycle.

Modeling tension stiffening as an axisymmetric problem required the prismatic specimens to be turned into equivalent cylinders, which was done by replacing the square section (80 × 80 mm) with a circular section of the same area ($\varnothing_c$ = 90 mm, Fig. 13a, b).

In the same figures the undeformed and deformed cross-sections (before loading and under loading, respectively) of a prismatic specimen and of the equivalent cylindrical specimen are sketched (Fig. 13a, b), together with the mean profile of the concrete strains assumed in the analysis of Specimen HPC/R/D/1, starting from the measured value ε_c^{exp}, that is the mean value over L'' (Fig. 9c), for $N/N_{max} = 95$ %. Note that in the analytical model, the strain along the perimeter of the circular section was given the same value ε_c^{exp} measured along the corners of the specimens.

5.2.3 Specimen HPC/R/D/1

In all the five specimens exhibiting tension stiffening, the bond stiffness was evaluated after heating to 640 °C, by means of a sort of back analysis. In the following, the Specimen HPC/R/D/1 is treated in some details for $N = 0.95\ N_{max} = 71$ kN (Fig. 11b). By giving k, E_s and E_c the following values at 640 °C: $k^{640} = 22$ MPa/mm; $E_s^{640} = 186.3$ GPa; $E_c^{640} = 6.2$ GPa, the diagrams of the internal forces $N_s^{640}(x)$, $N_c^{640}(x)$ and $V_B^{640}(x)$ were obtained (Fig. 14b–d; for the symbols see Fig. 14a).

In Fig. 14b the mean value of $N_s^{640}(x) = 63.3$ kN (= N_s^* dash-dotted line) is very close to the mean value $N_s^{AV} = 62.3$ kN (dashed line) obtained by multiplying the experimental mean strain ε_s^{AV} by E_s^{640} and A_s. The same occurs for the mean value of $N_c^{640}(x) = 7.5$ kN (= N_c^*), that practically coincides with the mean value $N_c^{AV} = 7.5$ kN (dashed line) obtained by multiplying the mean strain ε_c^{AV} by E_c^{640} and A_c.

Note that in any given section, the strain in the concrete depends on the distance r from the axis of the bar (Fig. 13c). Such a dependency was taken care of by assuming for ε_c an inverse proportionality with r (i.e., $\varepsilon_c \approx 1/r$), starting from the values measured along the longitudinal edges of the specimens. The agreement between the results yielded by the model (in terms of mean values of the axial forces in the bar, N_s^*, and in the concrete, N_c^*), and those yielded by testing (N_s^{AV}, N_c^{AV}) confirms that the value adopted for k^{640} (= 22 MPa/mm) is reliable. Furthermore, the low value of k^{640} (compared with the values inferred from the tests in ordinary conditions) was expected, as similar or lower values are reported in the literature [18]. It is worth noting that the secant slope of the $\tau_B - s$ curve given in CEB-FIP MC 90 [34] is comprised between 50 MPa/mm for $s \leq 0.4$ mm, and 200 MPa/mm for $s \leq 0.1$ mm, in ordinary environmental conditions. (In the following, the value $k = 110$ MPa/mm is adopted in ordinary environmental conditions, see Sect. 5.2.4).

In Fig. 14c, the axial forces in the bar and in the concrete after heating to 640 °C (N_s^{640} and N_c^{640}, thick curves), and in virgin conditions (no thermal damage, N_s^{20} and N_c^{20}, thin curves) are plotted as a function of the longitudinal coordinate x, according to the uniaxial slip-based model. Note the sizable decay of tension

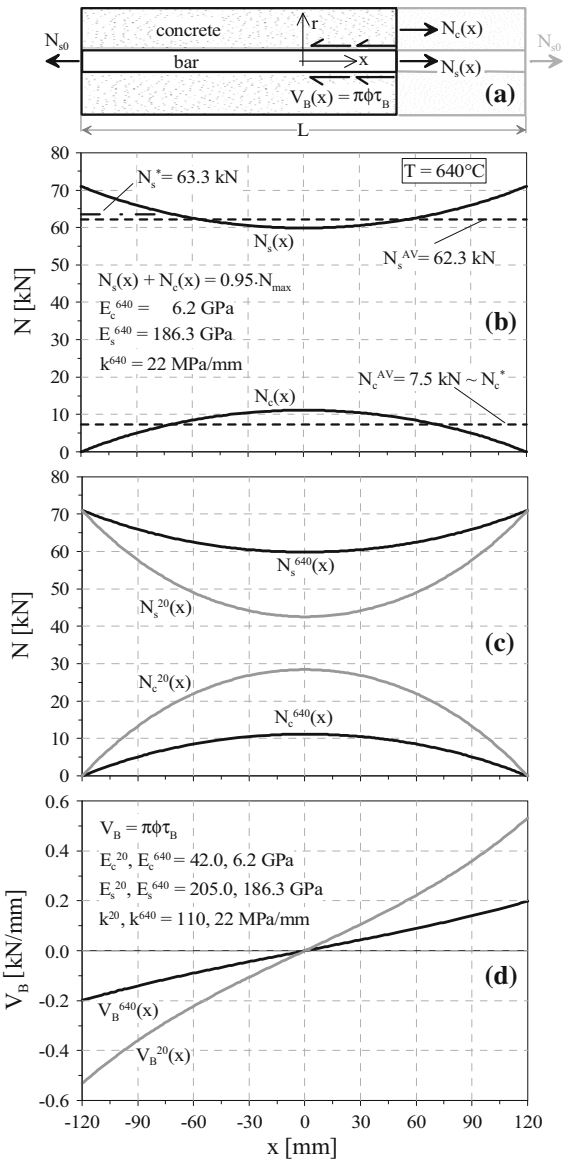

Fig. 14 Specimen HPC/R/D/1: **a** *symbol* and conventions; **b** diagrams of the axial forces in the *bar* $N_s^{640}(x)$ and in the concrete $N_c^{640}(x)$, and mean experimental values N_s^{AV} and N_c^{AV} (*dashed lines*) at 95 % of the maximum load N_{max} (N_{max} = load at steel yielding). The *dash-dotted line* is the mean theoretical value N_s^* of $N_s^{640}(x)$; **c** diagrams of the axial forces $N_s(x)$ and $N_c(x)$ after heating to 640 °C and in virgin conditions (no thermal damage); and **d** diagrams of the bond force per unit length $V_B(x)$ (N/mm), assuming $k^{20} = 110$ MPa/mm

stiffening from 20 to 640 °C, following the mechanical decay of bond (Fig. 14d). As a matter of fact, in ordinary environmental conditions, tension stiffening is very effective and in the mid-span section roughly 40 % of the load is resisted by the concrete, while after the exposure to 640 °C concrete carries not more than 15 % of the load. In Fig. 14d, the bond force per unit length $V_B = \pi \varnothing \tau_B$ [kN/mm] is plotted as a function of the longitudinal coordinate x, after a thermal cycle at 640 °C (black curve) and in virgin conditions (no thermal damage, grey curve). The much lower bond force at 640 °C results from the temperature-triggered mechanical decay of bond.

5.2.4 Bond stiffness as a function of the temperature

The bond stiffness k was evaluated in the five specimens exhibiting tension stiffening on the basis of the slopes of the stress–strain curves (Fig. 11a–e). According to the uni-dimensional slip-dependent model, by integrating Eq. 5 the ratio between the elastic modulus of embedded and naked bars (E^*/E_s) can be formulated as follows:

$$\frac{E_s^*}{E_s} = \frac{\varepsilon_s^{\text{nakedbar}}}{\varepsilon_s^{\text{embedbar}}} = \frac{\sigma_{s0}/E_s}{\varepsilon_s^{AV}} = \frac{\sigma_{s0}/E_s}{\frac{1}{E_s L}\left[\int_{-\frac{L}{2}}^{\frac{L}{2}} \sigma_s(x)\mathrm{d}x\right]} = \frac{1+n\rho}{\frac{2}{\lambda L}\cdot\tanh\left(\lambda\frac{L}{2}\right)+n\rho} = f(k). \quad (7)$$

By imposing f(k) to be equal to the experimental value of the ratio E_s^*/E_s (Fig. 11a–e), k can be numerically worked out. This procedure was applied to the five specimens in order to evaluate their bond stiffness, as a function of their residual compressive strength. (The compressive strength at 640 °C was evaluated by testing six specimens—two per each mix—obtained by cutting the least damaged unreinforced prisms past the thermal shock and the rest at 750 °C; $a \times b = 80 \times 80$ mm; $h = 160$ mm).

In particular:

- NSC (Specimen NSC/R/W/1): $k_{NSC}^{640} = 19$ MPa/mm for $f_c^{640} = 16$ MPa
- HPC (Specimens HPC/R/D/1, 2 and W/2): $k_{HPC}^{640} = 32$ MPa/mm for $f_c^{640} = 24$ MPa
- HSC (Specimen HSC/R/W/1): $k_{HSC}^{640} = 37$ MPa/mm for $f_c^{640} = 26$ MPa

The previous results suggest a simple linearity for the relationship between the bond stiffness k and the compressive strength of the concrete f_c, be it heat damaged or not (Fig. 15, Eqs. 8a or 8b):

$$k = 1.35 f_c \quad (8a)$$

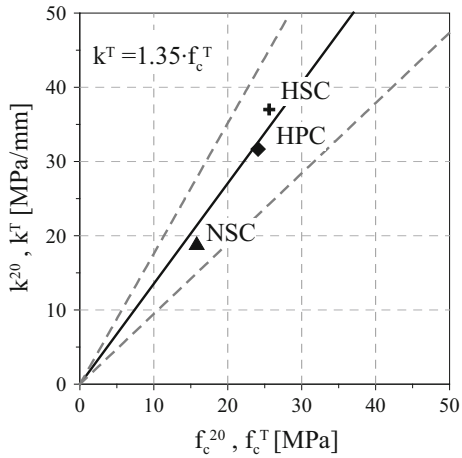

Fig. 15 Possible linear relationship between the bond stiffness and concrete compressive strength, with/without thermal damage; the symbols refers to the three mixes after heating to 640 °C

$$k^T/k^{20} = f_c^T/f_c^{20} \tag{8b}$$

According to Eq. 8a, the bond stiffness in virgin conditions for the three concretes examined in this project has the following values:

$k_{NSC}^{20} = 69$ MPa/mm;
$k_{HPC}^{20} = 110$ MPa/mm;
$k_{HSC}^{20} = 122$ MPa/mm,

which are in good agreement with the range 50–200 MPa/mm suggested by MC 90, for $s \leq 0.4$ mm and $s \leq 0.1$ mm, respectively.

As indicated by the three values of k concerning the HPC specimens ($k_{HPC}^{640} = 22$, 32 and 42 MPa/mm, average value 32 MPa/mm), the dispersion of the results is rather high for the same concrete and thermal conditions. Hence Eqs. 8a,b are merely indicative of a trend, and for any given concrete strength (and temperature) a dispersion of ±30 % has to be expected (see dashed lines in Fig. 15).

6 Conclusions

Concrete spalling at high temperature is a rather elusive phenomenon, as demonstrated by the tests performed in the first phase of this study, where a number of reinforced and unreinforced prismatic specimens made of three different self-compacting concretes were subjected to a severe thermal shock to induce corner spalling. A specific procedure was proposed as well, to make the tests on spalling as systematic as possible. Only a limited number of specimens exhibited medium spalling (10 %) or light spalling (10 %), something unexpected, whose reasons are still under scrutiny. One possible explanation may be that the relatively small size of the specimens prevented in most cases the formation of a *moisture clog*, even if the permeability of the adiabatic surfaces (not exposed to the heat) was greatly reduced by impregnating them with silicon layers, gluing steel barriers and adding insulating layers.

A second reason is certainly the lack of load-induced stresses and/or thermal self-stresses, the latter being small—or absent—because of the lack of geometric continuity along the adiabatic surfaces. (Comparing different cementitious mixes, however, requires simple, handy specimens, where spalling is mostly due to concrete intrinsic behavior and not to structural factors). Finally, the rather limited—but realistic—moisture content did not help, as well as the lack of certain additives like microsilica. The critical and still-open issue, however, seems to be whether any test procedure based merely on pore pressure and thermal gradients at high temperature be effective in producing a sizeable spalling, as required by the cross examination of different spalling-proof mixes.

As for the proposed set-up, both the preparation of the specimens and their introduction inside the furnace required simple and safe operations, compatible with the use of off-the-shelf furnaces.

In the second phase of this study, the reduction of tension-stiffening effectiveness after a thermal shock and a prolonged rest at high temperature was investigated. The preliminary results on tension stiffening presented in this paper shed some light on three aspects, that should be looked at more thoroughly:

- bond stiffness decreases sharply with the temperature, as it appears to be linearly related to the decay of the compressive strength; hence, after being exposed to temperatures in excess of 600 °C, at least a 3-times decrease of bond stiffness should be expected, and even more, like in the *reference case* developed in this study;
- for the geometry of the specimens tested in this project and for the three self-compacting mixes, assuming perfect elasticity for the materials (steel

and concrete) and for bond, up to 40 % of the applied load is transferred to concrete via bond in virgin conditions, while only 15–25 % is transferred after the exposure to 640 °C;

- in virgin conditions, the uniaxial slip-based model adopted in this study yields rather high values for the maximum bond stress (close to 1/7 f_c^{20}, not incompatible with self-compacting concrete), while both the model and the experimental results yield much lower maximum stresses after the exposure to 640 °C (but still close to 1/6 f_c^{640}); hence, even if these rather high values are mitigated by bond nonlinearity in actual embedded bars, the ratio of the maximum bond-stress value to the compressive strength tends to remain rather constant (close to 1/6–1/7 f_c), as if the heat-damaged concrete were simply a different lower-grade material, embracing a bar mostly unaffected by the heat.

Summing up, even during a severe fire, corner spalling (that is among the most dangerous types of spalling) may or may not occur, as pore pressure by itself is generally unable to activate an extended breaking-off of the concrete. Consequently, any test procedure devised to quantify concrete sensitivity to spalling—based only on concrete constitutive behavior—may be little effective, as thermal self-stresses and load-induced stresses are missing. Furthermore, the rather limited or even absent spalling in little stressed R/C members allows post-fire tension stiffening to be still effective, as bond stiffness appears to be a linear function of concrete strength in residual conditions. This is a rather unexpected finding, that should be taken care of in planning any repair activity past a fire in those structures requiring an appropriate stiffness even after such a severe event.

Acknowledgments The experimental campaign was jointly financed by CTG-Italcementi (Bergamo, Italy), which cast all the specimens, and by the Italian Ministry of Higher Education within the National Project "Optimization of Construction Methods and Materials in Tunnel Linings" (2007–2009). The authors would like to thank MS Candidates Alessandro Maggioni and Silvia Biancini, whose cooperation was instrumental in successfully performing the tests on spalling (2011) and tension stiffening (2012), respectively, in partial fulfilment of the requirements of their MS study plan in Civil Engineering, with a major in Structures. The authors are also grateful to Dr. Patrick Bamonte of DICA- Politecnico di Milano for his assistance in planning the tests and his valuable suggestions in the elaboration of the results.

References

1. Xi Y, Bažant ZP, Molina L, Jennings HM (1994) Moisture diffusion in cementitious materials. Adv Cem Based Mater 1:258–266
2. Khoury AG (2000) Effect of fire on concrete and concrete structures. Prog Struct Eng Mater 2:429–447
3. Dehn F, Koenders EAB (eds, 2009). Concrete spalling due to fire exposure. In: Proceedings of the 1st international workshop, published by Leipzig University, Leipzig, pp 548
4. Koenders EAB, Dehn F (eds, 2011). In: Proceedings of the 2nd international RILEM workshop on "Concrete Spalling due to Fire Exposure". RILEM Publications S.A.R.L., Delft. Oct 5–7, pp 433
5. Smith K, Atkinson TW (2009) Factors to consider in using PP fibres for explosive spalling resistance. In: Proceedings of the 1st international workshop on concrete spalling due to fire exposure, Dehn F, Koenders EAB (eds), published by Leipzig University, Leipzig, pp 364–373
6. Kodur VKR, Dwaikat MB (2009) Fire-Induced Spalling In Concrete—state-of-the-art and research needs. In: Proceedings of the 1st international workshop on concrete spalling due to fire exposure, Frank D, Koenders EAB (eds), published by Leipzig University, Leipzig, pp 248–268
7. Pimienta P, Pardon D, Mindeguia JC (2010) Fire behaviour of HPC—an experimental investigation on spalling risk. In: Proceedings of the 6th international conference "Structures in Fire"—SIF'10, Kodur VKR, Franssen JM (eds), DEStech Publ. Inc., East Lansing, pp 880–889
8. Kalifa P, Chéné G, Gallé C (2001) High-temperature behaviour of HPC with polypropylene fibres: from spalling to microstructure. Cem Concr Res 31:1487–1499
9. Jansson R, Boström L (2008) The influence of pressure in the pore system on fire spalling of concrete. In: Proceedings of the 5th international conference "Structures in Fire"—SIF'08, Tan KH, Kodur VKR, Tan TH (eds), publshed by Nanyang Tech. University, City of Singapore, pp 418–429
10. RILEM (1985). Properties of materials at high temperatures: concrete. Schneider U (ed), Department of Civil Engineering, University of Kassel, Kassel, pp 131
11. Lublóy E, Balázs GL (2012) Influence of high temperatures on bond. In: Proceedings of the 4th international conference" bond in concrete—BIC'2012". Cairns JW, Giovanni M, Plizzari GA, Brescia, pp 567–572. June 18–20, V.2
12. Sager H, Rostasy FS (1980). High temperature behavior of reinforcing and prestressing steels. Technical Universität Braunschweig, Sonderforschungs-Bereich 148, Part II, 51–53
13. ACI 216-1.07 (2007) Code requirements for determining fire resistance of concrete and masonry construction assemblies. Report by Joint ACI/TMS Committee 216, p 32
14. EN 1992-1-2:2004, Eurocode 2 (2004). Design of concrete structures. Part 1–2: General rules—structural fire design, European Committee for Standardization (CEN), Brussels
15. Felicetti R, Gambarova PG (2008) Expertise and assessment of materials and structures. fib Bulletin No. 46 "Fire Design of Concrete Structures—Structural Behaviour and Assessment", Luc T, Niels PH (eds), pp 63–114
16. EN 1994-1-2:2004, Eurocode 4 (2004). Design of composite steel and concrete structures. Part 1–2: General

rules—structural fire design, European Committee for Standardization (CEN), Brussels
17. Phan LT, Carino NJ (1998) Review of mechanical properties of HSC at high temperature. ASCE J Mater Civ Eng 10(1):58–64
18. El-Hawary MM, Hamoush SA (1996) Bond shear modulus of reinforced concrete at high temperatures. Eng Fract Mech 55(6):991–999
19. Chiang CH, Tsai CL (2003) Time-temperature analysis of bond strength of a rebar after fire exposure. Cem Concr Res 33:1651–1654
20. Haddad RH, Al-Saleh RJ, Al-Akhras NM (2008) Effect of elevated temperature on bond between steel reinforcement and fiber-reinforced concrete. Fire Saf J 43: 334–343
21. Haddad RH, Shannis LG (2004) Post-fire behavior of bond between high-strength concrete and reinforcing steel. Constr Build Mater 18:425–435
22. Bingöl AF, Gül R (2009) Residual bond strength between steel bars and concrete after elevated temperatures. Fire Saf J 44:854–859
23. Huang Z (2010) Modelling the bond between concrete and reinforcing steel in a fire. Eng Struct 32:3660–3669
24. Bamonte P, Gambarova PG (2012) A study on the mechanical properties of self-compacting concrete at high temperature and after cooling. Mater Struct. doi:10.1617/s11527-012-9839-9,13pp
25. Bamonte P, Gambarova PG, Maggioni A, Lo Monte F (2011) A proposal for an experimental set-up to investigate fire-induced corner damage in R/C members. In: Proceedings of the 2nd international RILEM workshop on "Concrete Spalling due to Fire Exposure", Eduard K, Frank D (ed), pp 369–376 Delft. 5–7 Oct
26. Bamonte P, Biancini S, Lo Monte F (2012) Preliminary results on tension stiffening in heat-exposed R/C tension members. In: Proceedings of the 4th international conference" bond in concrete—BIC'2012", Cairns JW, Giovanni M, Plizzari GA, Brescia. 18–20, June V.2, pp 559–565
27. Lo Monte F (2013) Spalling and tension stiffening in heat-exposed members made of self-compacting concrete. Studies and researches: annual review of structural concrete, Politecnico di Milano and Italcementi (eds), published by Imready, San Marino, V.32, 179–200
28. Jansson R, Boström L (2014) Fire spalling of concrete—A re-assessment of test data. In: Proceedings of the 8th international conference on structures in fire—SiF 2014, Shanghai. 11–13 June, V.1, 297–304
29. Tanibe T, Ozawa M, Kamata R, Uchida Y, Rokugo K (2014) Development and evaluation of a model for fire-related HSC spalling failure. In: Proceedings of the 8th international conference on structures in fire—SiF 2014, Shanghai. 11–13, June, V.1, 411–418
30. EN 1992-1-1:2004, Eurocode 2 (2004). Design of concrete structures. Part 1-1: General rules and rules for buildings, European Committee for Standardization (CEN), Brussels
31. Kalifa P, Menneteau FD, Quenard D (2000) Spalling and pore pressure in HPC at high temperatures. Cem Concr Res 30:1915–1927
32. Hou X, Kodur VKR, Zheng W (2014) Factors governing the fire response of bonded prestressed concrete continuous beams. Mater Struct. doi: 10.1617/s11527-014-0365-9
33. UNI 6556 (1978). Tests of concretes. Determination of static modulus of elasticity in compression, Italian Standard
34. CEB–FIP Model Code (1990) Comité Euro-International du Beton–Fédération International de la Précontrainte, Lausanne